Society For Biomaterials

Preparation and *in vivo* evaluation of multifunctional ^{90}Y-labeled magnetic nanoparticles designed for cancer therapy

Magdalena Radović,[1] María Pilar Calatayud,[2] Gerardo Fabián Goya,[2] Manuel Ricardo Ibarra,[2] Bratislav Antić,[1] Vojislav Spasojević,[1] Nadežda Nikolić,[1] Drina Janković,[1] Marija Mirković,[1] Sanja Vranješ-Đurić[1]

[1]"Vinča" Institute of Nuclear Sciences, University of Belgrade, PO Box 522, 11000 Belgrade, Serbia
[2]Instituto de Nanociencia de Aragón (INA), University of Zaragoza, Mariano Esquillor s/n, 50018 Zaragoza, Spain

Received 12 December 2013; revised 20 February 2014; accepted 5 March 2014
Published online 00 Month 2014 in Wiley Online Library (wileyonlinelibrary.com). DOI: 10.1002/jbm.a.35160

Abstract: Two different types of magnetic nanoparticles (MNPs) were synthesized in order to compare their efficiency as radioactive vectors, Fe_3O_4-Naked (80 ± 5 nm) and polyethylene glycol 600 diacid functionalized Fe_3O_4 (Fe_3O_4-PEG600) MNPs (46 ± 0.6 nm). They were characterized based on the external morphology, size distribution, and colloidal and magnetic properties. The obtained specific power absorption value for Fe_3O_4-PEG600 MNPs was 200 W/g, indicated their potential in hyperthermia based cancer treatments. The labeling yield, *in vitro* stability and *in vivo* biodistribution profile of ^{90}Y-MNPs were compared. Both types of MNPs were ^{90}Y-labeled in reproducible high yield (>97%). The stability of the obtained radioactive nanoparticles was evaluated in saline and human serum media in order to optimize the formulations for *in vivo* use. The biodistribution in Wistar rats showed different pharmacokinetic behaviors of nanoparticles: a large fraction of both injected MNPs ended in the liver (14.58%ID/g for ^{90}Y-Fe_3O_4-Naked MNPs and 19.61%ID/g for ^{90}Y-Fe_3O_4-PEG600 MNPs) whereas minor fractions attained in other organs. The main difference between the two types of MNPs was the higher accumulation of ^{90}Y-Fe_3O_4-Naked MNPs in the lungs (12.14%ID/g vs. 2.00%ID/g for ^{90}Y-Fe_3O_4-PEG600 MNPs) due to their *in vivo* agglomeration. The studied radiolabeled magnetic complexes such as ^{90}Y-Fe_3O_4-PEG600 MNPs constitute a great promise for multiple diagnostic-therapeutic uses combining, for example, MRI-magnetic hyperthermia and regional radiotherapy. © 2014 Wiley Periodicals, Inc. J Biomed Mater Res Part A: 00A:000–000, 2014.

Key Words: magnetic nanoparticles, ^{90}Y, PEG, hyperthermia, radionuclide therapy

How to cite this article: Radović M, Calatayud MP, Goya GF, Ibarra MR, Antić B, Spasojević V, Nikolić N, Janković D, Mirković M, Vranješ-Đurić S. 2014. Preparation and *in vivo* evaluation of multifunctional ^{90}Y-labeled magnetic nanoparticles designed for cancer therapy. J Biomed Mater Res Part A 2014:00A:000–000.

INTRODUCTION

Notable advances have been witnessed over the past decade on radiolabelling of nanovectors for diagnostic and therapeutic purposes. Multifunctional vectors capable of simultaneously deliver radionuclides, and concurrently provide imaging capability and therapeutic effect in the target tissue are highly desirable. With the capacity for a large dose of radioactivity inside each particle, nanoparticles can be very useful especially for internal cancer radiotherapy.[1] They could be delivered to tumor tissue by passive targeting taking advantage of the enhanced permeability and retention (EPR) effect of tumor tissues.[2,3] Nanometer sized biocompatible magnetic nanoparticles exhibiting enhanced retention by vascularized tumors are ideal for selective tumor accumulation. Their use was intended to improve the delivery of the radionuclides to the tumor as well as retention time of the radiation source in the target tissues under the force of an external magnetic field. Moreover, magnetic nanoparticles can be useful as thermoseeds for inducing hyperthermia. The synergistic interaction between hyperthermia and radiation therapy is based on the heat effect that may make some cancer cells more sensitive to radiation or harm other cancer cells that radiation cannot damage.

Because of inhomogeneous distribution of radiolabeled particles, especially within the large tumor with a necrotic center, long-range β-emitters like yttrium-90 (^{90}Y), holmium-166 (^{166}Ho), and rhenium-188 (^{188}Re) are proposed to be suitable candidates for internal radionuclide therapy, especially of primary and metastatic malignancies,[4] while alpha- and Auger-emitters, due to their short range in tissues, would be more appropriate for effective killing of circulating cells with minimal irradiation of the blood

Correspondence to: S. Vranješ-Đurić; e-mail: sanjav@vinca.rs
Contract grant sponsor: The Serbian Ministry of Education and Science; contract grant number: III 45015
Contract grant sponsor: The Spanish Ministerio de Economía y Competitividad (MINECO); contract grant numbers: MAT2010-19326 and HelloKit INNPACTO

vessels.[5–7] ^{188}Re was explored for labeling silica,[8] human serum albumin,[9] and polyacrylamide[10] coated magnetite nanoparticles for magnetically targeted radiotherapy.

^{90}Y is high energy β-emitter with optimal nuclear-physical characteristics (decay half-life 64.1 h, $E\max_{\beta}$ of 2.27 MeV) for radionuclide tumor therapy and can affect tumor cells up to a maximum depth of 11 mm in the soft tissue.[11] This is described by the cross fire effect occurring due to the long beta particles path that crosses multiple individual cells decreasing the need to target the each cancer cell with the radiopharmaceutical. ^{90}Y-labeled albumin microspheres with encapsulated citric acid-coated magnetite nanoparticles have been investigating for possible applications in a bimodal radionuclide-hyperthermia cancer therapy.[12] Since labeling with different radionuclides most often requires new optimization of the procedure, for our purpose ^{90}Y is the radionuclide of choice for MNPs-radiolabeling since it can be used for varied desirable purposes, from nanoparticles tracking to the possible application in radionuclide therapy.

In our ongoing study, we report synthesis, characterization, ^{90}Y-labeling and *in vitro* stability of naked MNPs and functionalized with PEG600-diacid polymers MNPs. The *in vivo* biodistribution was studied for both MNPs to assess the effect of different physicochemical characteristics on the biological fate of the particles. Dicarboxyl-terminated polyethylene glycol 600 (PEG600 diacid) is the good choice as a typical non-toxic, non-antigenic, and protein resistant polymer.[13] It can readily react with the iron metal ion and attach onto the Fe_3O_4 particle surface, providing the magnetic nanoparticle biocompatibility, meanwhile offering free surface carboxylate groups for further interactions with positively charged radionuclides.[14,15]

MATERIALS AND METHODS

Chemicals

All reagents were commercially available and used as received without further purification. Iron (II) sulfate heptahydrate ($FeSO_4{\cdot}7H_2O$), sodium hydroxide (NaOH), potassium nitrate (KNO_3), sulfuric acid (H_2SO_4), ferrous chloride tetrahydrate ($FeCl_2{\cdot}4H_2O$), ferric chloride anhydrous ($FeCl_3$), poly(ethylene glycol) bis(carboxymethyl) ether average M_n 600 (PEG600 diacid), and aqueous ammonia solution (25 %) were obtained from Sigma–Aldrich. Nitric acid 65% extra pure (HNO_3) from Merck was used. $^{90}YCl_3$ was purchased from Polatom, Poland, in a no-carrier-added form (29.64 GBq/cm^3, in 0.05 M HCl, 18.5 TBq/mg Y, according to the product specification).

Synthesis of Fe_3O_4-Naked MNPs

The synthesis protocol used was based on the well-known oxidative hydrolysis method, as described elsewhere.[16] In a typical synthesis, 1.364 g of KNO_3 and 0.486 g of NaOH were dissolved in 135 mL of distilled water in a three-necked flask bubbled with N_2. Then, 15 mL of 0.01 M H_2SO_4 solution containing 0.308 g of $FeSO_4{\cdot}7H_2O$ (previously flowed with N_2 for 2 h) was added dropwise under constant stirring. When the precipitation was completed, N_2 was allowed to pass for another 5 min and the suspension with the black precipitate was held at 90°C for 24 h under N_2. Afterward, the solution was cooled with an ice bath, and the resulting Fe_3O_4-precipitate was separated by magnetic decantation and washed several times with distilled water.

Synthesis of Fe_3O_4-PEG600 MNPs

These nanoparticles were synthesized by co-precipitation of ferric and ferrous salts in a basic solution.[17,18] Aqueous solutions (15 mL each) of 0.3 *M* $FeCl_2{\cdot}4H_2O$, 0.6 *M* $FeCl_3$, and 20 mL of 10% PEG600 diacid were mixed together and heated up to 50°C under continuous stirring. Then some dosage of ammonia solution was dropped until the pH of the mixture reached 10. The solution was vigorously stirred at 50°C for 1 h. The resulting Fe_3O_4-PEG600 precipitate were retrieved by centrifugation at 20,000 rpm for 30 min and washed several times with deionized water.

Experimental methods for characterization of MNPs

Transmission electron microscopy (TEM). MNPs average size, size distribution and morphology were analyzed by TEM using an FEI Tecnai T20 microscope operating at 200 kV and FEI Tecnai F30 microscope operated at an acceleration voltage of 300 kV. TEM samples of MNPs were prepared by placing one drop of a dilute suspension of MNPs in water on a carbon-coated copper grid and allowing the solvent to evaporate at room temperature.

Zeta potential. The zeta potential was evaluated at room temperature with a photo correlation spectrometer (PCS) Brookhaven 90 plus (Zetasizer Nano^{TM}, Malvern Instrument) from a dilute suspension of the sample in water in the presence of 0.01 *M* of KCl.

The hydrodynamic diameter distribution of the Fe_3O_4-PEG600 MNPs in their aqueous suspensions was obtained using a photo correlation spectrometer (PCS) Brookhaven 90 plus (Zetasizer Nano^{TM}, Malvern Instrument).

Thermogravimetric analysis (TGA). TGA of magnetic powder was measured using TGA/DSC 1 (Mettler Toledo). The analysis was designed at room temperature up to 900°C fixing a heating rate of 10°C min^{-1} under a continuous flux of nitrogen.

Fourier transform infrared spectroscopy (attenuated total reflectance mode) (FTIR). The FTIR spectrum was used to analyze functional groups of polymers/Fe_3O_4 nanoparticles and verify their presence on MNPs surface. The spectrum was taken from 4000 cm^{-1} to 400 cm^{-1} on a Nicolet Impact 410 spectrometer.

Magnetic measurements. Magnetic measurements were performed on MPMS XL-5 SQUID magnetometer. The magnetization vs. temperature, *M* (*T*) curves, were measured in the temperature range between 1.8 K and 300 K, applying zero-field-cooled (ZFC) and field-cooled (FC) measuring

protocols, in an applied field of 100 Oe. Hysteresis loops were measured at 5 K and 300 K in ZFC regimes.

Magnetic hyperthermia. To characterize the heating capability of the multifunctional magnetic vectors, alternating magnetic field (AMF) experiments were performed using a commercial applicator device (model DM100, nB Nanoscale Biomagnetics, Spain) at a frequency $f = 580$ kHz and amplitude $H = 23.8$ kAm^{-1}. To determine the specific power absorption (SPA) values of pure colloids, the temperature increase of 1 mL of each MNPs suspension (at concentration of 24 mg/mL) was measured using an optical fiber system dipped into the sample. The SPA values (measured in W per gram of MNPs) for each colloid were calculated from the initial slope of the ΔT versus time data and using the equation given in the Results section.

Determination of Fe_3O_4 content in MNPs. The Fe concentration was determined by VIS–UV transmission spectrophotometry (Shimadzu UV-160) using thiocyanate complexation through the following reaction[19]

$$Fe^{3+}{}_{(aq)} + 6\,SCN^{-}{}_{(aq)} \rightarrow \left[Fe\,(SCN)_6\right]^{3-}{}_{(aq)}$$

Fe_3O_4-naked and Fe_3O_4-PEG600 were dissolved in 1:1 v/v 6 *M* HCl/ HNO_3 (65%) at 50–60°C for 2 h, in order to dissolve the nanoparticles and oxidize the ferrous to ferric ions. Potassium thiocyanate was then added to the Fe^{3+} solution to form the iron–thiocyanate complex, which has strong absorbance at 478 nm wavelength. The iron concentration was determined by comparing the sample absorbance to a calibration curve.

Labeling of MNPs with ^{90}Y

Radiolabeling was performed by mixing 0.5 mL of aqueous Fe_3O_4-Naked and Fe_3O_4-PEG600 MNPs suspension with 37 MBq $^{90}YCl_3$ (0.001 mL) and incubating at room temperature on a shaker for 1 h. After synthesis and before addition of $^{90}YCl_3$ both suspensions of MNPs were washed several times with deionized water until pH 6.5 for Fe_3O_4-Naked and pH 5.5 for Fe_3O_4-PEG600, respectively. Radiolabeled particles were then separated from free ^{90}Y activity by precipitation with the help of permanent magnet. Supernatant was removed and precipitated ^{90}Y-labeled MNPs were washed with deionized water several times. The labeling yield of the ^{90}Y-MNPs was calculated (after magnetic decantation) as [radioactivity in the pallet/activity in the supernatant + activity in the pellet] × 100. Formation of ^{90}Y-labeled MNPs and radiochemical purity were verified by a radiochromatography analysis performed on silica-gel-impregnated glass-fiber sheets (SG) with saline as the mobile phase. With this system, ^{90}Y-labeled MNPs remain at the origin while unbound ^{90}Y migrates with the solvent front.

Stability testing of the ^{90}Y-labeled MNPs

To estimate the *in vitro* stability of ^{90}Y-labeled MNPs, samples of the final preparation of ^{90}Y-Fe_3O_4-Naked and

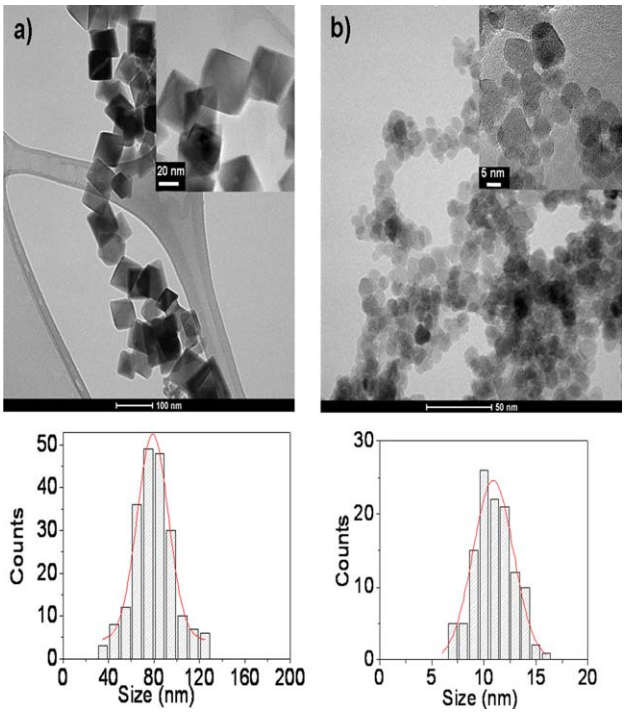

FIGURE 1. TEM images and histogram showing the particle size distribution of (a) Fe_3O_4-Naked MNPs and (b) Fe_3O_4-PEG600 MNPs. [Color figure can be viewed in the online issue, which is available at wileyonlinelibrary.com.]

^{90}Y-Fe_3O_4-PEG600 were incubated with 2 mL either saline solution (0.9% NaCl, pH = 7.3) or human serum at 37°C for 72 h. At various time intervals after the labeling (0.5, 1, 24, 48 and 72 h), the radiolabeled particles were magnetically precipitated and the activity was measured separately in a 0.1 mL aliquot of the supernatant and the remaining sample. These results were compared with radiochromatography analysis (on SG plates with saline as the mobile phase).

Biodistribution and *in vivo* stability of ^{90}Y-labeled MNPs

The biodistribution of both MNPs was evaluated following intravenous administration of 0.1 mL saline suspension of ^{90}Y-labeled MNPs (1.85 MBq) in healthy male Wistar rats (body mass 130–150 g, 5 weeks old). At five time points ($t = 0.5$, 1, 24, 48 and 72 h), groups of rats ($n = 3$–5 per each time point) were sacrificed and samples of blood and organs were excised, weighed, then tissues were homogenized (Bio Spec Products, Inc., Bartlesville, OK) and diluted to a final volume of 5 mL with water to reach identical geometry and similar probe density. The "bremsstrahlung" of ^{90}Y radioactivity was measured by a CRC-15 beta radioisotope dose calibrator (Capintec, USA) and well type NaI (Tl) gamma counter (WallacCompu Gamma Counter LKB, Finland). The percentage of injected activity per gram (%ID/g) of organ was calculated by comparing the activities with appropriate standards for injected dose (ID). The data are presented as average ± standard deviation from each group. The entire animal study conformed to ethical guidelines and the rules for animal care proposed by the

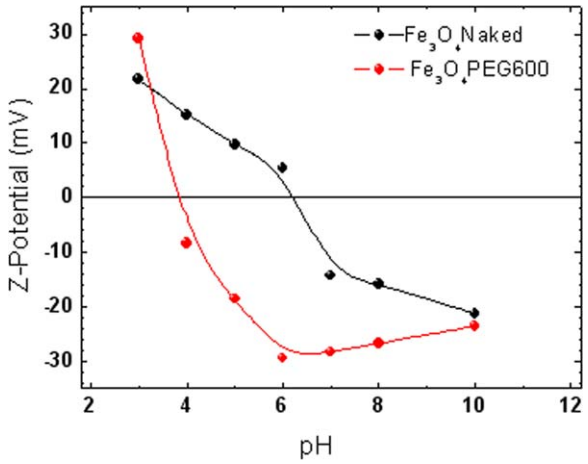

FIGURE 2. Zeta potential data of Fe_3O_4-Naked MNPs and Fe_3O_4-PEG600 MNPs in pure water by varying the pH. [Color figure can be viewed in the online issue, which is available at wileyonlinelibrary.com.]

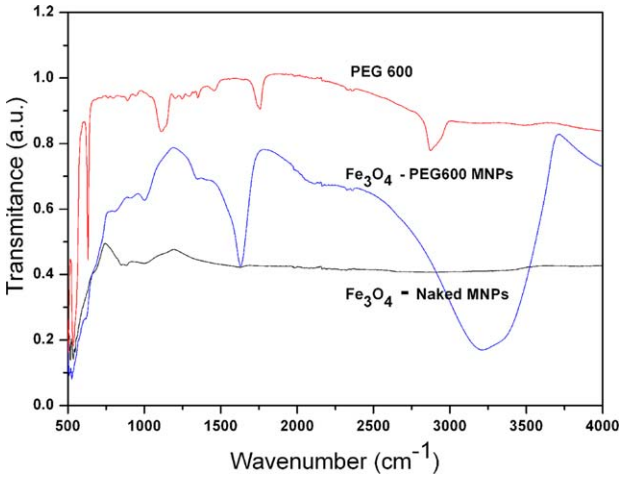

FIGURE 3. FTIR spectra of Fe_3O_4-Naked MNPs, Fe_3O_4-PEG600 MNPs, and pure PEG600 diacid polymer. [Color figure can be viewed in the online issue, which is available at wileyonlinelibrary.com.]

Serbian Laboratory Animal Science Association (SLASA) which complied with Directive 2010/63/EU of the European Parliament and of the Council on the protection of animals used for scientific purposes.

RESULTS AND DISCUSSION

Synthesis and characterization of the MNPs

Iron oxide nanoparticles were prepared by two different methods, Fe_3O_4-Naked MNPs by an oxidative hydrolysis of ferrous sulfate with NaOH[16] and Fe_3O_4-PEG600 MNPs by precipitation from ferrous/ferric chloride solutions.[20] In the first method, ferrous hydroxide suspension is oxidized with KNO_3. Fe_3O_4-Naked MNPs of average sizes 80 ± 5 nm which were not stable due to their big size were obtained (Fig. 1a). The other method consists in aging stoichiometric mixtures of ferrous and ferric hydroxides in aqueous media, yielding spherical magnetite particles of 10 ± 1.9 nm (Fig. 1b). In this case, PEG600 diacid was added during the nanoparticles synthesis in order to functionalize them. The presence of the polymer on nanoparticles surface determines the surface charge, their resistance to aggregation, and provide available functional groups for further functionalization. From TEM images it can be seen that the Fe_3O_4-Naked MNPs display an octagonal morphology, as expected for the crystal magnetite. The PEG-coated MNPs, on the other side, displayed a more spherical morphology.

The hydrodynamic diameter of Fe_3O_4-PEG600 MNPs obtained from dynamic light scattering (DLS) measurements was d_{hyd} 46 ± 0.6 nm, reflecting the effect of the coating polymer layer on the 10 nm magnetic cores obtained from TEM images. The free polymeric chains of this surface coating extended into the water from the surface of the magnetic cores. These results confirm the binding of PEG600 molecules onto the iron oxide nanoparticles[21] and small degree of aggregation in the water-based colloid.

The MNPs surface charges were assessed through measurements of the zeta potential of their aqueous suspensions as a function of pH (Fig. 2). The changes in the surface charge potential of Fe_3O_4-Naked MNPs in water with various pH values could be explained by protonation–deprotonation of surface hydroxyl groups (Fe–OH).[22] The unmodified Fe_3O_4-Naked MNPs precipitate from their aqueous suspension, which suggests that the zeta potential of -14.64 mV at pH 7 is not enough to achieve stable suspension. Binding of PEG600 diacid generate highly negative surface charge of Fe_3O_4-PEG600 MNPs (-28 mV at pH 7) providing electrostatic repulsion between MNPs, therefore stable suspension was achieved. Also, compared to the isoelectric point (IEP) of Fe_3O_4-Naked MNPs (6.2), IEP of Fe_3O_4-PEG600 MNPs is reduced to 3.8. These results suggest that some of the carboxylate groups of PEG600 diacid strongly coordinate to iron cations on iron oxide surface while uncoordinated carboxylate groups exposed to the solvent, should be responsible for making the surface charged.[21,23,24]

Further confirmation of effective coating of the PEG600 diacid on the surface of MNPs came from FTIR spectroscopy and thermogravimetric analysis. Figure 3 shows FTIR spectra of Fe_3O_4-Naked MNPs, Fe_3O_4-PEG600 MNPs, and pure PEG600 diacid polymer.

The strong absorption band at 580 cm^{-1} is the characteristic absorption of the Fe–O linkages of MNPs, observed in the infrared spectra of iron oxide nanoparticles with and without a PEG600 coating, confirmed that the main phase of iron oxide in both samples was magnetite.[25] The large and intense band at approximately 3209 cm^{-1} could be assigned to the structural OH groups as well as to the traces of molecular water. The peaks at 1752 cm^{-1} and 1453 cm^{-1} corresponding to stretching vibration of C=O and bending vibration of OH of PEG diacid were shifted to lower frequencies 1634 cm^{-1} and 1417 cm^{-1} in Fe_3O_4-PEG600 spectrum. The result demonstrated that the coordinate bond was formed between carboxylate groups of PEG and iron cations of Fe_3O_4, the peaks of C=O and OH were equalized to two peaks, 1417 cm^{-1} peak was symmetrical stretching vibration of C=O, 1634 cm^{-1} peak was asymmetric stretching vibration of

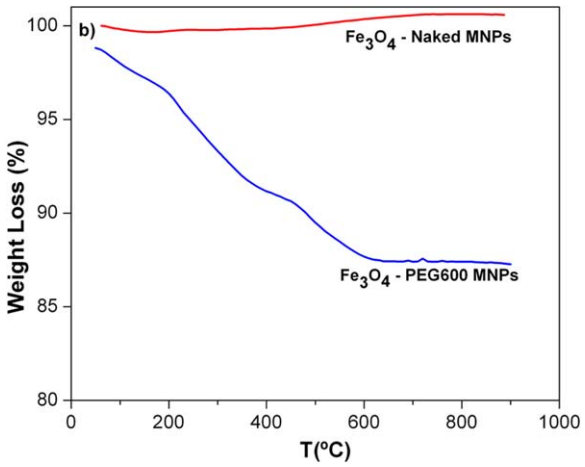

FIGURE 4. TGA curves of Fe_3O_4-Naked MNPs and Fe_3O_4-PEG600 MNPs. [Color figure can be viewed in the online issue, which is available at wileyonlinelibrary.com.]

C=O.[26,27] Generally, carboxylate group may be bound to a metal cation in a monodentate, bidentate (chelating) or bridging fashion. The coordination type can be interpreted from the wavenumber separation Δ between the asymmetric and symmetric stretching bands. A monodentate ligand is expected at $\Delta > 200$ cm^{-1} and a bidentate at $\Delta < 110$ cm^{-1}. According to the reported results, $\Delta \approx 217$ cm^{-1} for PEG diacid-coated MNPs infers monodentate fashion.[28]

TGA tests disclose the amount of PEG600 attached to the surface of the MNPs (Fig. 4). A continuous weight loss is observed in the temperature range of 200–600°C because of the decomposition of PEG600 coated on the nanoparticles. In this temperature range, the total weight loss is 12% Fe_3O_4-PEG600 MNPs. No more weight loss is found from 600 to 900°C indicative of a complete burning of the surface ligand.[14]

Thus, the zeta potential, FTIR, and TGA results confirmed that Fe_3O_4 nanoparticles have been functionalized probably by coordinating via one of carboxylate groups from PEG diacid and there will be one carboxylate group

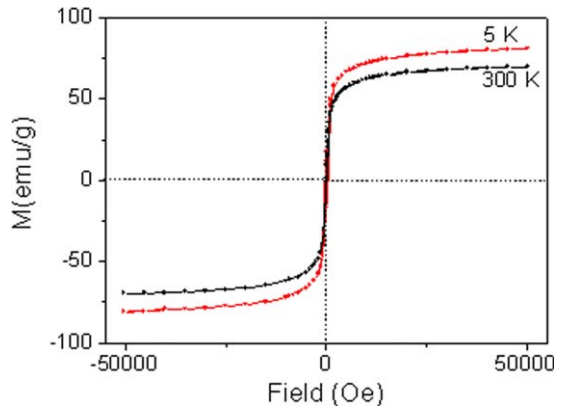

FIGURE 5. Hysteresis loop for Fe_3O_4-PEG600 MNPs. [Color figure can be viewed in the online issue, which is available at wileyonlinelibrary.com.]

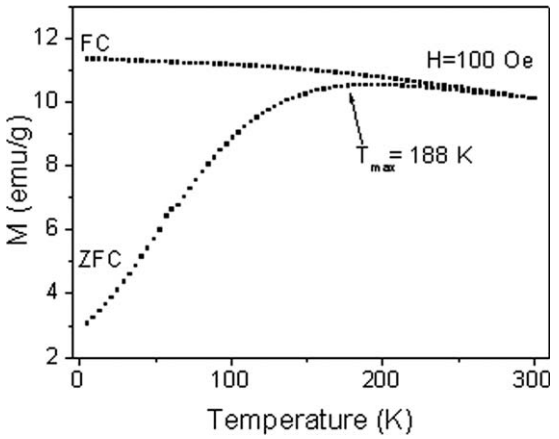

FIGURE 6. Temperature dependence on magnetization of the Fe_3O_4-PEG600 MNPs taken in zero-field and field-cooling modes.

exposed to the solvent that should be responsible for the surface charge. The presence of this negatively charged terminal carboxylate group provides an avenue to extended bond formation with positively charged ^{90}Y.

DC magnetization, hysteresis loop, and SPA measurements

The magnetic response of Fe_3O_4-PEG600 MNPs is illustrated in Figure 5. The saturated magnetization (M_s) values are 70 and 79 emu/g at 300 K and 5 K, respectively, similar to the previously reported values for naked MNPs[16] (77 emu/g at 250 K). The hysteresis loop at 300 K shows superparamagnetic behavior with negligible coercivity (H_C) ($H_C < 25$ Oe) and the zero value of the remanence (M_R).

Consistently, the ZFC-FC curves show that the blocking temperature of Fe_3O_4-PEG600 MNPs is located at $T = 188$ K, well below room temperature (Fig. 6). In the case of naked MNPs the blocking temperature above room temperature is in agreement with their large size.[16]

The heating capacity of the Fe_3O_4-PEG600 MNPs under applied ac magnetic field ($H = 23.8$ kAm^{-1} and $f = 580$ kHz), was measured from the initial slope of the T vs. time curves (Fig. 7) from which the specific power absorption (SPA) values were calculated using the following equation:

$$\mathrm{SPA} = C_c \rho_c (\Delta T/\Delta t)/\Phi$$

where C_c is the specific heat capacity of the solvent; ρ_c, the density of the solvent; and Φ, the weight concentration of MNPs, as assessed by thiocyanate colorimetry. The obtained SPA value for Fe_3O_4-PEG600 MNPs was 200 W/g, which indicates that these MNPs can be used as heating agents for *in situ* magnetic fluid hyperthermia protocols. SPA value of Fe_3O_4-Naked MNPs was not determined due to instability of the sample.

In order to compare SPA values from different experimental setups, the field- and frequency dependence of this parameter has to be taken into account (as proposed by Kallumadil et al.[29]) by the use of the intrinsic loss power (ILP) parameter, (SPA/[$H^2 \cdot f$]). The ILP provides a physical

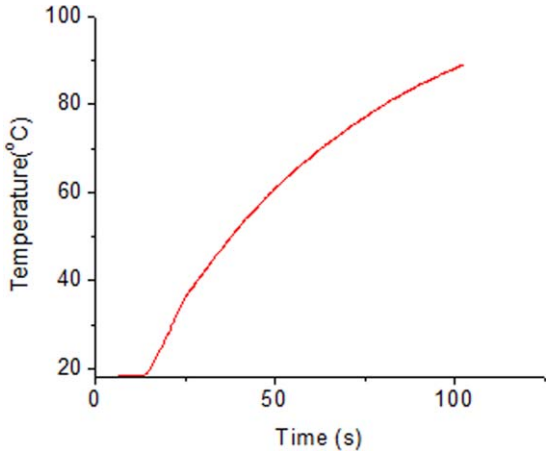

FIGURE 7. The heating curves of Fe_3O_4-PEG600 MNPs. [Color figure can be viewed in the online issue, which is available at wileyonlinelibrary.com.]

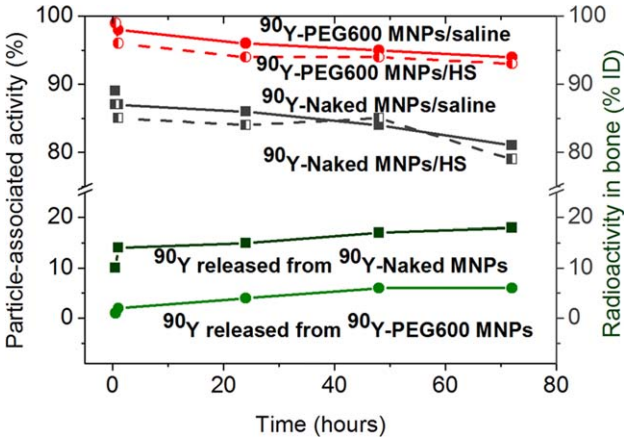

FIGURE 8. Stability studies of ^{90}Y-Fe_3O_4-Naked MNPs and ^{90}Y-Fe_3O_4-PEG600 MNPs in saline and human serum (HS) up to 72 h and *in vivo* stability of ^{90}Y-labeled MNPs determined from the measured radioactivity in bone. [Color figure can be viewed in the online issue, which is available at wileyonlinelibrary.com.]

magnitude that is independent of the experimental setup, so the frequencies of the experiments are within the LF range (i.e., approx. <800 kHz) and the amplitude satisfy $H \ll H_C$.

Previous works by de la Presa et al.[30] on similar magnetite based ferrofluids reported values from 50 to 58 W/g for uncoated magnetic nanoparticles of sizes ranging between 11 and 15 nm, at 7.5 kAm^{-1} and $f = 522.3$ kHz. The smaller value obtained in this work, as compared to ours, is in very good agreement with the expected quadratic field-dependence of the SPA ratio that can be expressed as

$$\frac{\mathrm{SPA}\,(H_1)}{\mathrm{SPA}\,(H_2)} = \frac{f_1 \times H_1^2}{f_2 \times H_2^2} \cong 3.9$$

where H_1, f_1 and H_2, f_2 are the magnetic field amplitudes and frequencies used in this study and in the work of de la Presa et al.,[30] respectively.

Labeling of MNPs with ^{90}Y

The radiotracer technique is the most effective method that can be used to quantify the accumulation of MNPs in *in vivo* and *in vitro* systems. There are currently some limitations on the methods which can be used to radiolabel a particle. Binding of the radionuclide to a nanoparticle have to be irreversible to prevent their escape to other tissues or organs and the manufacturing process is time limited and difficult because of the risk of contamination. Once the radiolabeling method for the selected radionuclide and nanoparticle is optimized, radioactive part in the newly radiolabeled compound could be used not only for nanoparticles tracking but also for radiodiagnosis or radiotherapy.[31–34]

The major requirements of this method are that the labeling process does not significantly alter the structure or properties of the nanoparticles and that the stability of radiolabeled product is sufficiently high to allow further *in vitro* and *in vivo* studies. Magnetite is a widely used nanoparticles and their radiolabeling open up the possibility to quantify the extremely small amounts of these nanoparticles in complex biological systems.[35] As mentioned above, in aqueous solutions the Fe atoms coordinate with water, which dissociates readily to leave the iron oxide surface hydroxyl functionalized. Dependent upon the pH of the solution, the surface of the magnetite will be positive or negative.[15,35] In an acidic environment, the hydroxyl groups at the surface of the iron oxide are doubly protonated ($\equiv FeOH_2^+$) and the surface charge of the iron oxide is thus positive while at pH values above the IEP (6.2), the hydroxyl group is deprotonated ($\equiv FeO^-$), and consequently the iron oxide surface bears a negative charge.[22] Based on this, we supposed the possible labeling of partially deprotonated Fe_3O_4-Naked MNPs with $^{90}Y^{3+}$ at the pH above 6.2. ^{90}Y-labeling of Fe_3O_4-Naked MNPs was successfully achieved at pH 6.5. Addition of small volume of $^{90}YCl_3$ insignificantly changed the pH of the labeling mixture, so the influence on the Fe_3O_4-Naked MNP properties was not expected. Labeling yields determined by measurement of radioactivity in MNPs precipitate after magnetic separation as well as by radiochromatography analysis exceeded 97%.

For Fe_3O_4-MNPs coated with PEG600 diacid, the origin of surface charge changes with carboxylate groups, which can be neutral (CO_2H) or dissociate to CO_2^-.[22] High negative values of the zeta potential at pH 5.5 for Fe_3O_4-PEG600 MNPs due to the carboxylate-rich surface is suitable for labeling with positively charged $^{90}Y^{3+}$ therefore labeling resulted in very high labeling yield, 99%.

Stability studies

The results of measuring of the nanoparticles-associated radioactivity after magnetic precipitation as well as radiochromatography analysis showed that Fe_3O_4-PEG600 MNPs exhibited excellent *in vitro* stability both in saline and human serum over a 72 h period (Fig. 8).

After 72 h of incubation in saline and human serum, ^{90}Y-Fe_3O_4-Naked MNPs demonstrated a much lower stability

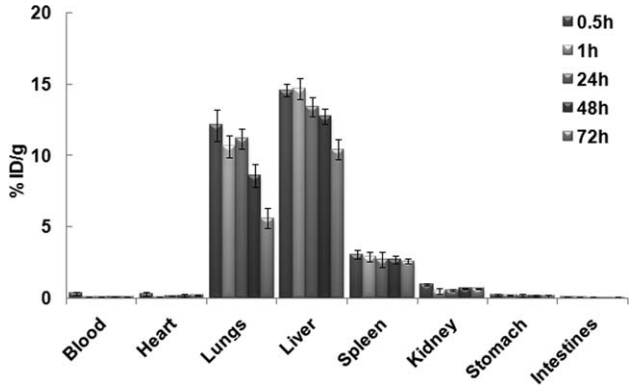

FIGURE 9. Biodistribution of ^{90}Y-Fe_3O_4-Naked MNPs in different tissues after 0.5, 1, 24, 48, and 72 h of intravenous administration in normal Wistar rats. The results are expressed as %ID/g organ (mean five rats ± standard deviations).

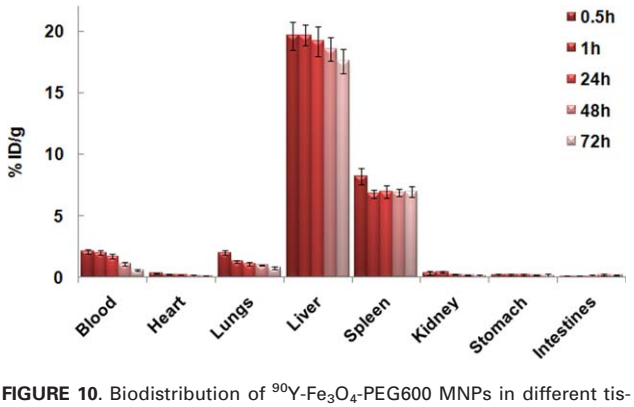

FIGURE 10. Biodistribution of ^{90}Y-Fe_3O_4-PEG600 MNPs in different tissues after 0.5, 1, 24, 48, and 72 h of intravenous administration in normal Wistar rats. The results are expressed as %ID/g of the organ (mean five rats ± standard deviations). [Color figure can be viewed in the online issue, which is available at wileyonlinelibrary.com.]

(81.3% and 78.6%, respectively) than ^{90}Y-Fe_3O_4-PEG600 MNPs (94.1 % and 93.2%, respectively). The percentage of injected dose in bone correlates with results of *in vitro* stability studies and confirmed that ^{90}Y-labeled Fe_3O_4-PEG600 MNPs were *in vivo* stabile. 6.1%ID in the bone 72 h after injection indicates significant *in vivo* stability of ^{90}Y-labeled Fe_3O_4-PEG600 MNPs in relation to ^{90}Y-Fe_3O_4-Naked MNPs (18.6%ID) since any ^{90}Y released from radiolabeled particles will get accumulated in the bone. The higher stability observed for ^{90}Y-Fe_3O_4-PEG600 MNPs could be attributed to the binding of $^{90}Y^{3+}$ by negatively charged carboxylate groups present on PEG600 MNPs surface.[36–38]

In contrast to the visible agglomeration of ^{90}Y-Fe_3O_4-Naked MNPs at physiological pH no *in vitro* agglomeration of the radiolabeled Fe_3O_4-PEG600 MNPs was observed during 10 days. Negative charge on the surface of Fe_3O_4-PEG600 MNPs provide strong electrostatic repulsion between MNPs, resulting in excellent solubility and stability of Fe_3O_4-PEG600 MNPs in aqueous solution as well as in physiological saline, human serum, and *in vivo*. Additionally, the chain of PEG diacid offered dimensional protection reducing the agglomeration among the particles and its hydrophilic groups made MNPs disperse providing good colloidal stability of the suspension at physiological pH.

In vivo biodistribution studies

The biodistribution and the final fate of intravenously injected particles are highly dependent on their physicochemical properties such as particle size, morphology, coating, and surface charge.[39,40] Particles with a diameter ranging from 10 to 100 nm optimal for intravenous injection demonstrate the most prolonged blood circulation times as well as penetrate the very small capillaries within the body tissues.[41] These particles are able to pass the fenestration in the liver and may be able to target the hepatocytes, although most are still taken up by the liver's Kupffer cells.[42] We followed intravenously injected ^{90}Y-labeled Naked and PEGylated nanoparticles size of 80 ± 5 nm and 46 ± 0.6 nm, respectively, with the aim to reveal their biodistribution profile and *in vivo* stability in healthy Wistar rats.

^{90}Y-labeled Fe_3O_4-Naked MNPs accumulated mostly in the liver (from 14.58%ID/g at the first 30 min after intravenous injection to 10.43%ID/g at 72 h) with additional substantial uptake in the lungs (from 12.14%ID/g at the first 30 min after injection to 5.35%ID/g at 72 h) (Fig. 9). High liver and lung uptake was expected by observing the results of *in vitro* instability of nanometer sized Fe_3O_4-Naked MNPs. Because of the large surface area to volume ratio, the magnetic nanoparticles tend to agglomerate and adsorb plasma proteins consequently resulting in rapid clearance from circulation. The body's reticuloendothelial system, mainly the Kupffer cells in the liver, usually takes up these nanoparticles due to the hydrophobic surface.[43] Their high accumulation in the form of micrometric agglomerates in the lung is based mainly on the particle size achieved by agglomeration. It was reported that micrometer sized particles were accumulated almost entirely in the lung in the first pass of circulation through the pulmonary artery following intravenous administration.[12]

Agglomeration behavior could be minimized by tailoring a suitable surface coating or drug delivery vehicle. Several reports give evidence that surface functionalization of magnetite nanoparticles leads to improved drug delivery and circulation by minimizing particle agglomeration.[44] The surface functionalization of magnetite nanoparticles with hydrophilic polymeric surfactants such as PEG600 diacid is expected to prevent these phenomena.[40] Biodistribution of ^{90}Y-Fe_3O_4-PEG600 MNPs in Wistar rats showed that ^{90}Y-Fe_3O_4-PEG600 MNPs were mainly accumulated in liver, 19.61%ID/g at the first 30 min after intravenous injection, followed by spleen 8.20%ID/g and lungs 2.00%ID/g (Fig. 10). These nanoparticles displayed long-term retention especially in liver: 19.17%ID/g was retained in the liver after 24 h and even 17.56%ID/g remained 72 h post injection there. Unfortunately, even after coating by PEG diacid, phagocytic cells of the liver and spleen were able to recognize and clear invading ^{90}Y-Fe_3O_4-PEG600 MNPs. The main difference between the two types of magnetic nanoparticles was the higher accumulation of ^{90}Y-Fe_3O_4-Naked MNPs in the lungs. Surface coverage by PEG600 over the nanoparticles enhances surface

hydrophilicity of MNPs preventing agglomeration to micrometer sized particles and therefore affects their fate *in vivo*.[45] Besides decreased lungs uptake, PEGylation significantly increased the blood circulation time from 0.51%ID (^{90}Y-Fe_3O_4-Naked MNPs) to 2.12%ID (^{90}Y-Fe_3O_4-PEG600 MNPs).

These results show importance of PEGylation of Fe_3O_4 in terms of increasing *in vivo* stability and their long-term retention in one organ. Intra-arterial or direct intratumoral injection of ^{90}Y-labeled Fe_3O_4-PEG600 MNPs could be applied in combined endoradiotherapy-hyperthermia treatment especially for liver tumors. *In vivo* stability and long-term retention of ^{90}Y-Fe_3O_4-PEG600 MNPs in liver could allow repeated and concentrated hyperthermia treatments in the same area leading to increased perfusion in the tumor region, therefore higher radionuclide delivery and more effective radiotherapy.

CONCLUSIONS

We report here, for the first time, the design and preparation of multifunctional ^{90}Y-labeled MNPs with potential ability to perform concurrent tracking, imaging and therapeutic application *in vivo*. The Fe_3O_4-PEG600 MNPs are phase purity with good morphological and magnetic properties. They displayed superparamagnetic behavior at room temperature with saturated magnetization, M_s of 70 emu/g. The obtained SPA value for Fe_3O_4-PEG600 MNPs was 200 W/g, which indicates that these MNPs can be used as heating agents for *in situ* magnetic fluid hyperthermia protocols. The product of the magnetic field and the frequency applied in these case $H{\cdot}f = 3.9 \times 10^9$ A m^{-1} s^{-1} ($H = 23.8$ kA m^{-1} and $f = 580$ kHz), is within the acceptable range for a safe application of hyperthermia to patients.

^{90}Y-labeling of both Fe_3O_4-Naked and Fe_3O_4-PEG600 MNPs has demonstrated to be a precise method for studies of uptake, distribution, and biodegradation of magnetite particles *in vivo*. Besides, high labeling yield and *in vitro* and *in vivo* stability of labeled PEGylated magnetite nanoparticles create opportunities for their use as a multifunctional diagnostic and therapy agents. Due to significant uptake of ^{90}Y-Fe_3O_4-PEG600 MNPs in liver and their low uptake by other tissues, MNPs labeled with beta-emitters could be suitable for use as treatment agents for liver malignancies. Also, if applied intratumorally the large portion of the same radiolabeled preparations is expected to retain in the tumor with a small percentage entering the systemic circulation. These results seemed to be promising for the potential use of radiolabeled PEGylated magnetite nanoparticles in the combined radiotherapy-hyperthermia cancer treatment.

REFERENCES

1. Mitra A, Nan A, Line BR, Ghandehari H. Nanocarriers for nuclear imaging and radiotherapy of cancer. Curr Pharm Des 2006;12: 4729–4749.
2. Maeda H, Wu J, Sawa T, Matsumura Y, Hori K. Tumor vascular permeability and the EPR effect in macromolecular therapeutics: a review. J Control Release 2000;65:271–284.
3. Tanaka T, Shiramoto S, Miyashita M, Fujishima Y, Kaneo Y. Tumor targeting based on the effect of enhanced permeability and retention (EPR) and the mechanism of receptor-mediated endocytosis (RME). Int J Pharm 2004;277:39–61.
4. Nijsen JF, van het Schip AD, Hennink WE, Rook DW, van Rijk PP, de Klerk JM. Advances in nuclear oncology: microspheres for internal radionuclide therapy of liver tumours. Curr Med Chem 2002;9:73–82.
5. Miederer M, Seidl C, Beyer GJ, Charlton DE, Vranjes-Duric S, Comor JJ, Huber R, Nikula T, Apostolidis C, Schuhmacher C, Becker KF, Senekowitsch-Schmidtke R. Comparison of the radiotoxicity of two alpha-particle-emitting immunoconjugates, terbium-149 and bismuth-213, directed against a tumor-specific, exon 9 deleted (d9) E-cadherin adhesion protein. Radiat Res 2003; 159:612–620.
6. Beyer GJ, Miederer M, Vranjes-Durić S, Comor JJ, Künzi G, Hartley O, Senekowitsch-Schmidtke R, Soloviev D, Buchegger F. Targeted alpha therapy in vivo: direct evidence for single cancer cell kill using 149Tb-rituximab. Eur J Nucl Med Mol Imaging 2004; 31:547–554.
7. Fani M, Vranjes S, Archimandritis SC, Potamianos S, Xanthopoulos S, Bouziotis P, Varvarigou AD. Labeling of monoclonal antibodies with 153Sm for potential use in radioimmunotherapy. Appl Radiat Isot 2002;57:665–674.
8. Cao J, Wang Y, Yu J, Xia J, Zhang C, Yin D, Häfeli UO. Preparation and radiolabeling of surface-modified magnetic nanoparticles with rhenium-188 for magnetic targeted radiotherapy. J Magn Magn Mater 2004;277:165–174.
9. Chunfu Z, Jinquan C, Duanzhi Y, Yongxian W, Yanlin F, Jiajü T. Preparation and radiolabeling of human serum albumin (HSA)-coated magnetite nanoparticles for magnetically targeted therapy. Appl Radiat Isot 2004;61:1255–1259.
10. Zhang C, Sun H, Xia J, Yu J, Yao S, Yin D, Wang Y. Synthesis of polyacrylamide modified magnetic nanoparticles and radiolabeling with 188Re for magnetically targeted radiotherapy. J Magn Magn Mater 2005;293:193–198.
11. Häfeli UO. Radioactive magnetic microspheres. In: Arshady R, editor. Radiolabeled and Magnetic Particulates in Medicine and Biology, MMI Series. vol. 3. London: Citus Books; 2001. p 559–584.
12. Radović M, Vranješ–Durić S, Nikolić N, Janković D, Goya G, Torres T, Calatayud P, Bruvera I, Ibarra R, Spasojević V, Jančar B, Antić B. Development and evaluation of ^{90}Y-labeled albumin microspheres loaded with magnetite nanoparticles for possible applications in cancer therapy. J Mater Chem 2012;22: 24017–24025.
13. Feng B, Hong RY, Wang LS, Guo L, Li HZ, Ding J, Zheng Y, Wei DG. Synthesis of Fe_3O_4/APTES/PEG diacid functionalized magnetic nanoparticles for MR imaging. Colloids Surf A Physicochem Eng Asp 2008;328:52–59.
14. Ge Q, Su J, Chung TS, Amy G. Hydrophilic superparamagnetic nanoparticles: synthesis, characterization, and performance in forward osmosis processes. Ind Eng Chem Res 2011;50:382–388.
15. Gil S, Castro E, Mano JF. Synthesis and characterization of stable dicarboxylic pegylated magnetite nanoparticles. Mater Lett 2013; 100:266–270.
16. Riggio C, Calatayud MP, Hoskins C, Pinkernelle J, Sanz B, Torres TE, Ibarra MR, Wang L, Keilhoff G, Goya GF, Raffa V, Cuschieri A. Poly-l-lysine-coated magnetic nanoparticles as intracellular actuators for neural guidance. Int J Nanomed 2012;7:3155–3166.
17. Massart R, Cabuil V. Effect of some parameters on the formation of colloidal magnetite in alkaline medium. J Chim Phys 1987;84: 967–973.
18. Lee J, Isobe T, Senna M. Preparation of Ultrafine Fe_3O_4 Particles by Precipitation in the Presence of PVA at High pH. J Colloid Interface Sci 1996;177:490–494.
19. Gupta AK, Gupta M. Cytotoxicity suppression and cellular uptake enhancement of surface modified magnetic nanoparticles. Biomaterials 2005;26:1565–1573.
20. Verges MA, Costo R., Roca AG, Marco JF, Goya GF, Serna CJ, Morales MP. Uniform and water stable magnetite nanoparticles with diameters around the monodomain-multidomain limit. J Phys D Appl Phys 2008;41:134003 (10 pp).
21. Lu Q, Wei D, Zhou J, Xu J, Cheng J, Zhu J. Preparation of polymer-functionalized iron oxide nanoparticles and their biomedical properties. Chin J Chem 2013;31:401–406.

22. Yu S, Chowa GM. Carboxyl group ($–CO_2H$) functionalized ferrimagnetic iron oxide nanoparticles for potential bio-applications. J Mater Chem 2004;14:2781–2786.
23. Tobio M, Gref R, Sanchez A, Langer R, Alonso MJ. Stealth PLA-PEG nanoparticles as protein carriers for nasal administration. Pharmaceutical Res 1998;15:270–275.
24. Zhou YF, Du LR, Zhou C, Fan TY. Preparation and characterization of ferromagnetic fluids modified by carboxyl PEG. J Chin Pharm Sci 2012;21:50–56.
25. Závišová V, Koneracká M, Múčková M, Lazová J, Juríková A, Lancz G, Tomašovičová N, Timko M, Kováč J, Vávra I, Fabián M, Feoktystov AV, Garamus VM, Avdeev MV, Kopčanský P. Magnetic fluid poly(ethylene glycol) with moderate anticancer activity. J Magn Magn Mater 2011;323:1408–1412.
26. Gupta AK, Wells S. Surface-modified superparamagnetic nanoparticles for drug delivery: preparation, characterization, and cytotoxicity studies. IEEE Trans Nanobiosci 2004;3:66–73.
27. Nigam S, Barick KC, Bahadur D. Development of citrate-stabilized Fe_3O_4 nanoparticles: conjugation and release of doxorubicin for therapeutic applications. J Magn Magn Mater 2011;323:237–243.
28. Hu F, MacRenaris KW, Waters EA, Liang T, Schultz-Sikma EA, Eckermann AL, Meade TJ. Ultrasmall, water-soluble magnetite nanoparticles with high relaxivity for magnetic resonance imaging. J Phys Chem C 2009;113:20855–20860.
29. Kallumadil M, Tada M, Nakagawa T, Abe M, Southern P, Pankhurst QA. Suitability of commercial colloids for magnetic hyperthermia. J Magn Magn Mater 2009;321:1509–1513.
30. de la Presa P, Luengo Y, Multigner M, Costo R, Morales MP, Rivero G, Hernando A. Study of heating efficiency as a function of concentration, size, and applied field in γ-Fe_2O_3 nanoparticles. J Phys Chem B 2012;116:25602–25610.
31. Jankovic D, Vranješ-Đurić S, Djokic D, Markovic M, Ajdinovic B, Jaukovic LJ, Nikolic N. 90Y-labeled tin fluoride colloid as a promising therapeutic agent: preparation, characterization, and biological study in rats. J Pharm Sci 2012;6:2194–2203.
32. Nikolić N, Vranješ-Đurić S, Janković D, Đokić D, Mirković M, Bibić N, Trajković V. Preparation and biodistribution of radiolabeled fullerene C60 nanocrystals. Nanotechnology 2009;20: 385102 (7 pp).
33. Locatelli E, Gil L, Israel LL, Passoni L, Naddaka M, Pucci A, Reese T, Gomez-Vallejo V, Milani P, Matteoli M, Llop J, Lellouche JP, Franchini MC. Biocompatible nanocomposite for PET/MRI hybrid imaging. Int J Nanomed 2012;7:6021–6033.
34. Bouziotis P, Psimadas D, Tsotakos T, Stamopoulos D, Tsoukalas C. Radiolabeled iron oxide nanoparticles as dual-modality SPECT/MRI and PET/MRI agents. Curr Top Med Chem 2012;12: 2694–2702.
35. Laurent S, Forge D, Port M, Roch A, Robic C, Vander Elst L, Muller RN. Magnetic iron oxide nanoparticles: synthesis, stabilization, vectorization, physicochemical characterizations, and biological applications. Chem Rev 2008;108:2064–2110.
36. Wadas TJ, Wong EH, Weisman GR, Anderson CJ. Coordinating radiometals of copper, gallium, indium, yttrium, and zirconium for PET and SPECT imaging of disease. Chem Rev 2010;110:2858–2902.
37. Liu S. The role of coordination chemistry in the development of target-specific radiopharmaceuticals. Chem Soc Rev 2004;33: 445–461.
38. Chong HS, Milenic DE, Garmestani K, Brady ED, Arora H, Pfiester C, Brechbiel MW. In vitro and in vivo evaluation of novel ligands for radioimmunotherapy. Nucl Med Biol 2006;33:459–467.
39. Shanehsazzadeh S, Oghabian MA, Daha FJ, Amanlou M, Allen BJ. Biodistribution of ultra small superparamagnetic iron oxide nanoparticles in BALB mice. J Radioanal Nucl Chem 2013;295: 1517–1523.
40. Gonçalves C, Ferreira MF, Santos AC, Prata MI, Geraldes CF, Martins JA, Gama FM. Studies on the biodistribution of dextrin nanoparticles. Nanotechnology 2010;21:295103.
41. Gupta AK, Gupta M. Synthesis and surface engineering of iron oxide nanoparticles for biomedical applications. Biomaterials 2005;26:3995–4021.
42. Patil GV. Biopolymer albumin for diagnosis and in drug delivery. Drug Dev Res 2003;58:219–247.
43. Mahmoudi M, Simchi A, Imani M, Häfeli UO. Superparamagnetic iron oxide nanoparticles with rigid cross-linked polyethylene glycol fumarate coating for application in imaging and drug delivery. J Phys Chem B 2009;113:8124–8131.
44. Pablico-Lansigan MH, Situ SF, Samia AC. Magnetic particle imaging: advancements and perspectives for real-time in vivo monitoring and image-guided therapy. Nanoscale 2013;5:4040–4055.
45. Saatchi K, Häfeli UO. Radiolabeling of biodegradable polymeric microspheres with [99mTc(CO)3]+ and in vivo biodistribution evaluation using MicroSPECT/CT imaging. Bioconjug Chem 2009; 20:1209–1217.